Exploiting novel sterilization techniques for porous polyurethane scaffolds

Serena Bertoldi[1,2] · Silvia Farè[1,2] · Håvard Jostein Haugen[3] · Maria Cristina Tanzi[1,2]

Received: 1 December 2014 / Accepted: 30 March 2015

1 Introduction

Among the candidate materials for the fabrication of scaffolds for tissue regeneration, polyurethanes (PUs), with a broad range of chemical and physical characteristics, occupy an important position [1, 2]. Thanks to their excellent biocompatibility and blood compatibility, segmented thermoplastic PUs have been used since the 1960s for the production of biomedical implants, such as catheters, heart valves and vascular prostheses [3]. In tissue engineering (TE), PUs are of particular interest as they can be easily fabricated in porous structures and produced with stiff and/or elastomeric properties according to the specific functions they are designed for [4, 5]. Therefore, in the last years increasing attention was paid to porous PU structures, in particular for bone [4–8] and cartilage [9–11] regeneration, produced with different fabrication techniques [4]. During the last 10 years we set up a gas foaming process to prepare crosslinked PU foams with slow degradation rate and with a controlled range of pore size, open porosity and mechanical properties [12, 13]. PU foams with different hydrophilicity and calcium-phosphate loaded composites were also developed and characterized [14]. The in vitro cytocompatibility of the proposed PU foams was assessed using Saos-2 and MG63 cell lines [13, 15, 16], and mesenchymal stem cells (MSCs) isolated from human bone marrow [16] and from human term placenta [17].

As for any other biomedical device, sterilization of scaffolds is required to avoid risks of infection after in vivo implantation, but the sterilization treatment may adversely affect material properties [18]. Hence, it is important that the

✉ Serena Bertoldi
serena.bertoldi@polimi.it

[1] Department of Chemistry, Materials and Chemical Engineering “G. Natta”, Politecnico di Milano, P.zza Leonardo da Vinci 32, 20133 Milan, Italy

[2] Local Unit Politecnico di Milano, INSTM, Milan, Italy

[3] Department of Biomaterials, Institute for Clinical Dentistry, University of Oslo, Blindern, PO Box 1109, NO-0317 Oslo, Norway

Table 1 Components in the polyol mixture and their main properties

Component	Functionality	OH number (mgKOH/g)	MW (Da)
Desmophen® 10WF18 (Bayer)	2.7	27.6	5500
Desmophen 7619 W (Bayer)	≈3	128.8	–
Desmophen® 4051B (Bayer)	≈4	467.4	480
Butandiol (Sigma-Aldrich)	2	1245.0	–
Ethylene glycol (EG, Sigma-Aldrich)	2	1810.0	–
Potassium acetate in EG	–	1810.0	–
DABCO 33-LV (air products)	–	560.0	–

applied sterilization method does not adversely modify chemical and mechanical properties, as well as functionality and biocompatibility. In fact, given the nature of their action, the sterilization agent used in the different sterilization procedures can attack the polymer structure resulting in hydrolysis, oxidation, melting, chain scission and depolymerization [19, 20]. Focusing on PUs, different studies in the scientific literature showed that the sterilization method, both traditional (e.g. steam, ethylene oxide, and γ irradiation) and advanced (plasma and ozone), can modify the PU bulk and surface properties and alter their physico-chemical stability [19–24]. The majority of works reported in literature have been mostly based on the analysis of bulk materials, however the effects of sterilization could be different depending on the device morphology, being even more significant on porous structures compared to compact ones. Hence, the evaluation of the effects of sterilization on porous scaffolds is mandatory for their possible use in clinical practice. Despite this need, the scientific literature lacks in works focused on this aspect. PU porous structures have been sterilized by different methods, such as low temperature cycle ethylene oxide (EtOx) [1, 25–31], UV irradiation [27], γ irradiation [21, 32, 33], low-temperature plasma with vapour phase hydrogen peroxide [23, 34, 35] and ozone [34]. Plasma and ozone sterilization, for instance, are currently used to decontaminate disposables and biomedical devices; compared to the traditional techniques, they are easy, fast, cold and low-cost, with no toxic residuals to be eliminated [18, 23, 34, 36].

In particular, De Nardo et al. [23, 34] studied the modifications induced by plasma and ozone sterilization on shape memory polyurethane (SMP) foams, Haugen et al. [21, 32] assessed the effects of γ irradiation dose on the properties of polyether–urethane scaffolds, while Andrews et al. [27] evaluated surface topography and in vitro cytocompatibility of Tecoflex® SG-80A polyurethane electrospun scaffolds after ethylene oxide and UV-ozone sterilization.

In this work, polyurethane foams synthesized by gas foaming were sterilized with two advanced sterilization techniques, plasma (Sterrad® method, Advanced Sterilization Products, Johnson & Johnson) and ozone (125L Ozone Sterilizer, TSO_3), investigating then any modifications of their morphological, chemico-physical and mechanical properties. Possible release of low molecular weight products, impairing PU foam cell interaction, was evaluated by in vitro indirect cytotoxicity tests.

2 Materials and methods

2.1 PU foam synthesis

A PU foam was synthesized with a previously described one step bulk polymerization method [13, 16, 17], using water as expanding agent and iron–acetylacetonate (FeAA) as catalyst. Briefly, the polyol mixture was ad hoc prepared using the reagents listed in Table 1.

FeAA (0.001 % w/w_{polyol}), distilled water (2 % w/w_{polyol}) and the appropriate amount of isocyanate (stoichiometric ratio of OH/NCO = 100/73), methylene diphenyl diisocyanate prepolymer (Desmodur® PF, Bayer, Germany; −NCO = 23.0 ± 0.5 %) were added to the polyol mixture and mixed with a mechanical stirrer. The reaction mixture was stirred for 60 s and then poured into a custom-made poly(methylmethacrylate) mold (V = 500 cm^3). The mold was firmly closed by the use of screws, and the expanding reaction was allowed to take place at room temperature (RT) [12, 13]. The foam was extracted from the mold after 72 h and the superficial compact skin was removed to obtain a homogeneous porous structure. Finally, the foam was post-cured at RT for 7 days. The synthesized PU foam was purified by a 48 h immersion in absolute ethanol at RT, and subsequently carefully dried in air at RT before characterization.

2.2 PU foam sterilization

Specimens of the PU foam were subjected either to plasma (*pl*) or ozone (*oz*) sterilization. Foam specimens (Ø = 6 mm, h = 4 mm) underwent plasma sterilization by Sterrad® system (100S, Advanced Sterilization Products, Johnson & Johnson) according to the standard manufacturer procedures and clinical practice (IRCCS Istituto Nazionale per lo Studio e la Cura dei Tumori, Milano, Italy). Briefly, a 400 W radio-frequency power (RF,

13.56 MHz) is applied at a pressure of 500 mTorr, after injection of vaporized hydrogen peroxide (H_2O_2, 2 mg/L), to generate the plasma phase. H_2O_2 produces destructive hydroxyl free radicals which can attack membrane lipids, DNA and other essential cell components with inactivation of microorganisms, depending on sterilization parameters (e.g., time, temperature and H_2O_2 concentration) [19]. The overall plasma sterilization cycle lasts about 55 min, and occurs at temperature between 45 and 55 °C. The by-products of the process are water and oxygen, that do not need for aeration or ventilation, and hydrogen peroxide residuals are non-toxic and non-carcinogenic [18, 34].

Ozone sterilization was performed by using a TSO_3 system (125L, TSO_3 Inc. Québec, QC, Canada) at the Institut de Cardiologie de Montréal (Montréal, QC, Canada). In this system, medical grade oxygen is released into the ozone-generating unit and then subjected to an electrical field, which converts oxygen into ozone. Ozone is then fed into a humidified sterilization chamber and is subsequently reverted into oxygen using an ozone converting catalyst. The residues at the end of the sterilization cycle are oxygen and clean water vapor [37]. The process lasts about 4 h 30 min, at a temperature between 31 and 36 °C.

2.3 Morphological characterization

2.3.1 Scanning electron microscopy observation

The morphology of non sterilized (*ns*), plasma (*pl*) and ozone (*oz*) sterilized specimens (Ø = 6 mm, h = 4 mm) was investigated by Scanning Electron Microscope (SEM EVO50EP, Zeiss) at 15–18 kV and working distance 7.5–12 mm. The samples were mounted on aluminum stubs, lined with carbon pads and gold sputter-coated (Sputter Coater S150B, Edwards) before SEM observation. The images were acquired at 30 and ×100 magnification.

2.3.2 Micro computed tomography

Porosity, average pores size, pores size distribution and pores interconnection were evaluated by micro computed tomography (micro CT) analysis using a 1172 micro CT imaging system (Skyscan, Aartselaar, Belgium) at 4 µm voxel resolution, 173 µA X-ray tube current, and 60 kV voltage without any filters. The specimens (n = 3; Ø = 6 mm, h = 4 mm) were rotated through 180° around the long axis of the sample, with a rotation of 0.4°. The projection radiographs of the sample were reconstructed to serial coronal-oriented tomograms using a 3D cone beam reconstruction algorithm, setting the beam hardening to 20 % and the ring artifact reduction to 12. Tridimensional reconstruction of the internal pore morphology was carried out using axial bitmap images and analyzed by CTan software (Skyscan, Aartselaar, Belgium). The grey scale threshold was set between 55 and 230, removing all objects smaller than 400 voxels and not connected to the 3D model. To eliminate potential edge effects, the cylindrical volume of interest (VOI) was selected in the center of the specimen (Ø = 2.5 mm, h = 2 mm). Scaffold porosity was then calculated as:

$$Porosity = 100\,\% - vol\%\ of\ binarised\ object\ (scaffold\ material)\ in\ VOI \quad (1)$$

The mean pore diameter distribution was determined by measuring the material thickness on the inverse model, generated by setting the grey scale threshold between 0 and 45. All images underwent a 3D analysis, following a "shrink-wrap" function, which allowed measuring in a specimen the fraction of the pore volume that was accessible from the outside through openings of a certain minimum size [38]. A shrink–wrap process was performed between two 3D measurements to shrink the outside boundary of the VOI in a scaffold through any openings whose size is equal to or larger than a threshold value. Interconnectivity was calculated as follows:

$$Interconnectivity = \frac{V - V_{shrink-wrap}}{V - V_m} \times 100 \quad (2)$$

where V is the total volume of the VOI, $V_{shrink-wrap}$ is the VOI volume after shrink-wrap processing, and V_m is the volume of the sample material. The interconnective pore size is hereby called "cut-off pore diameter".

2.4 Physical characterization

2.4.1 Density

Density analyses were performed on *ns*, *pl* and *oz* specimens (n = 5; Ø = 15 mm, h = 10 mm). Foam density was evaluated according to EN ISO 845 standard practice, by weighing and measuring the specimens after conditioning for 24 h at 25 °C.

2.4.2 Water uptake

Water uptake tests were performed on *ns*, *pl* and *oz* specimens (n = 3; Ø = 15 mm, h = 10 mm). Dried samples were immersed in deionized water at 37 °C; at each time-point (0.5, 2, 6, 24, 96 and 240 h) specimens were drawn from the water, wiped with filter paper to remove liquid in excess, and weighed. The water uptake (W.U. %) was calculated according to the formula (3):

$$W.U.\,\% = \frac{W_t - W_0}{W_0} \times 100 \quad (3)$$

where W_o is the dry weight and W_t is the wet weight at the time-point t.

2.5 Chemical characterization

FT-IR analysis (Nicolet FT-IR 6700, Thermo Electron Corporation) was performed in the ATR mode, using an ATR Single Bounce accessory and a ZnSe crystal. The analyses were performed on *ns*, *pl* and *oz* specimens to evaluate possible structural modifications induced by the sterilization treatments. Three different points were chosen for each sample (1–3 mm thick) to verify the homogeneity of possible chemical modifications occurring upon sterilization. Peak height analysis was performed on the absorption bands listed in Table 2, corresponding to the characteristic absorption frequencies of PU soft and hard segments, according to the literature [39–41]. All the considered characteristic bands were normalized to the 1597 cm^{-1} band of the stretching absorption of aromatic (C=C), which was considered to be the internal reference, assuming that the aromatic rings of methylene diphenyl diisocyanate in the hard segments are not affected by degradation [42, 43]. Hydrogen-bonded and free carbonyl bands of urethane groups were determined by peak deconvolution of the 1780–1680 cm^{-1} region using the Peak Fitting Module® of Origin® v.8.5 (OriginLab®) software.

2.6 Mechanical characterization

To evaluate the possible influence of the sterilization process on the compressive properties of the PU foam, mechanical tests were carried out on *ns*, *pl* and *oz* samples (n = 3; Ø = 15 mm, h = 10 mm) according to the standard practice UNI 6350-38. Uniaxial mechanical tests were performed with an Instron model 4200 instrument, at a crosshead rate of 1 mm/min, with 1 N preload, in wet condition, i.e. by maintaining the specimens in distilled water at 37 °C for all the test time in a home-made thermostatic chamber. In addition, the specimens were previously soaked in distilled water up to the plateau value of their water uptake. One hysteresis cycle was performed for each sample: the compressive load was applied up to 50 % deformation and then removed to 0 % deformation. Tangent modulus (E), collapse modulus (m), stress and strain at the yield point (σ', ε'), stress at 10 % deformation ($\sigma_{10\ \%}$) and at 50 % deformation ($\sigma_{50\ \%}$) and the hysteresis area, related to energy dispersion, were drawn from the stress–strain curve elaboration. Figure 1 shows a representative stress–strain curve of a PU foam, and the mechanical parameters obtained by the analysis.

2.7 In vitro cytotoxicity test

The possible release of low molecular weight cytotoxic substances from the PU foam after sterilization was investigated by indirect cytotoxicity tests on *ns*, *pl* and *oz* specimens (n = 3; Ø = 6 mm, h = 4 mm). The in vitro cytotoxicity of the extracts was assessed using the MG63 human osteosarcoma cells line (ECACC No. 86051601). Extracts were obtained according to the standard practice UNI EN ISO 10993-5. PU *ns* samples were disinfected in 70 % v/v ethanol solution for 30 min, carefully washed with sterile water, and then exposed to UV light (10 min for each side, λ = 254 nm). Three specimens for each sample type (i.e., *ns*, *pl* and *oz* specimens) were immersed in Eagle's minimum essential medium (EMEM) additioned with 10 % fetal bovine serum (FBS) and 1 % penicillin/streptomycin, with a ratio material/medium of 0.04 $cm^3 \times ml^{-1}$. After 3 and 7 days of incubation, the medium extracts were put in contact with MG63 cells (cell density = 1×10^5 cells/well) in a 48-well tissue culture plate (TCPS) up to 48 h. Cells cultured in EMEM on TCPS were used as control. Cell viability was assessed using Alamar Blue™ (Serotec) colorimetric assay. After 48 h, the culture medium was replaced with 500 µl Alamar Blue™ solution (10 % v/v in culture medium) and the plate incubated for 4 h. Alamar Blue is a redox indicator, i.e. it responds to reduction or oxidation of the surrounding medium. In this assay it both fluoresces and changes color in response to the chemical reduction of culture medium that results from cell growth and proliferation. For each specimen, three replicates (100 µl each) of the medium were removed from each well, transferred to a 96 well plate and the absorbance measured using a Tecan Genius Plus plate reader (test wavelength: 570 nm; reference wavelength: 630 nm). Measured absorbance was expressed as relative ratio over control cells on TCPS.

2.8 Statistical analysis

Statistical analysis (Origin 7.0 software) was performed using a t test (Student test), with significance level

Table 2 Considered bands for peak height IR analysis of the PU foams

Wavenumbers (cm^{-1})	Assignments
3317-07	ν(N–H), H bonded
1730	ν(C=O), non-H-bonded carbonyl from urethane
1703	ν(C=O), H-bonded carbonyl from urethane
1597	ν(C=C), benzene ring
1100	ν(C–O–C), ether

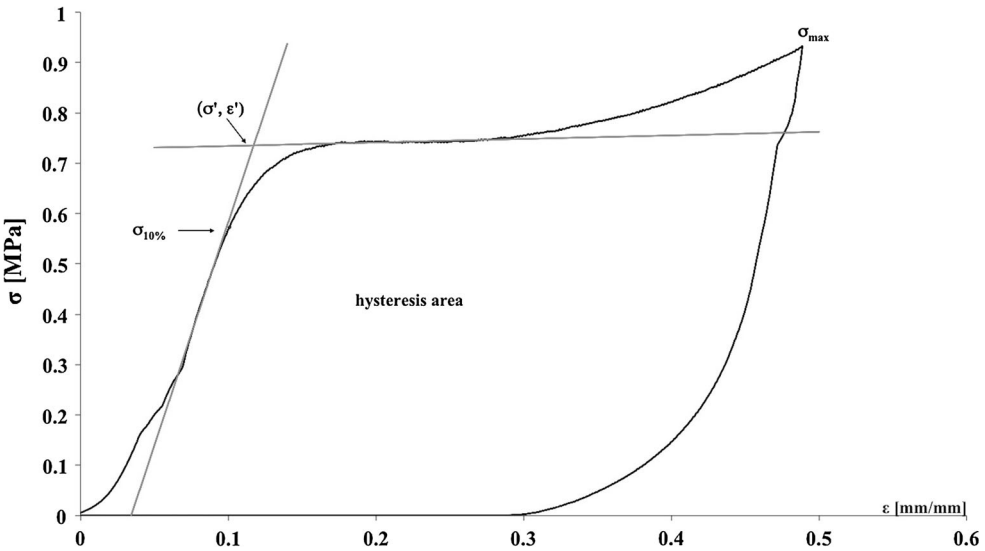

Fig. 1 Representative stress–strain curve and considered mechanical parameters obtained by uniaxial compressive test of PU foams

$P = 0.05$. Normal distribution was verified by normal probability plots.

3 Results

3.1 Morphological characterization

The morphology of the non sterilized and sterilized samples observed by SEM is shown in Fig. 2 (representative images). All the specimens presented homogeneous morphology with regular round-shaped pore size and distribution. Compared to the *ns* samples (Fig. 2a), a modification of the morphology of the foam was observed after sterilization (Fig. 2b–c). In particular, by observing SEM images, the ozone sterilization process (Fig. 2c) appeared to cause an increase of pore interconnection, as more pore channels were qualitatively detected than in *ns* and *pl* samples.

The morphological characterization carried out by micro CT partially confirmed the results obtained by SEM. The open porosity seems not to be affected by plasma and ozone sterilization, as no significant differences ($P > 0.05$) were detected among *ns*, *pl* and *oz* samples (Table 3). On the contrary, the average pores size significantly decreased ($P < 0.05$) after ozone sterilization, varying from 310 μm for *ns* specimens to 222 μm for *oz* ones (Table 3). Plasma sterilization had no influence ($P > 0.05$) on the average pore size.

Micro CT analysis also highlighted the effect of ozone sterilization on the average pore size distribution (Fig. 3a). Although plasma sterilization did not alter the average pore size distribution, showing a similar trend for pore size distribution curves of *ns* and *pl* specimens, ozone sterilization lead to the formation of new small pores, as suggested by the peak at about 150 μm, not detectable for *ns* and *pl* specimens.

No difference in pore interconnection was detected between the non sterilized foam and the specimens undergone plasma and ozone sterilization (Fig. 3b), as the pattern of accessible porosity as a function of cut off diameter for the three samples showed the same trend. Pore interconnection, in terms of accessible porosity, was about 50 % for the cut off diameter of 30 μm. In other words, considering pores with diameter ≤30 μm, the 50 % of the void volume (i.e. pore volume) was accessible and interconnected to the surface of the specimens.

3.2 Physical characterization

Both plasma and ozone sterilization treatments did not affect the foam density (Table 3) of the PU foam samples, as the differences among them were not statistically significant ($P > 0.05$).

Comparing the water uptake values of *ns* with *pl* specimens, no significant differences ($P > 0.05$) were observed for all the considered time points, except for 96 h of immersion. On the contrary, if compared to *ns* and *pl* specimens, significantly higher values of W.U. % ($P < 0.05$) were detected for *oz* samples for all the considered time points (Fig. 4). This result can be related to an increase of material hydrophilicity after ozone treatment, probably due to surface oxidation of the polyurethane structure and to the variation in pore size distribution detected by micro-CT.

3.3 Infrared characterization

Figure 5 shows the IR spectra in the range 4000–600 cm^{-1} (Fig. 5a) and 2000–1300 cm^{-1} (Fig. 5b) for *ns*, *pl* and *oz* PU foam specimens. On the whole, some differences before and after sterilization treatments were detected. In fact, after both plasma and ozone sterilization, the peak of the

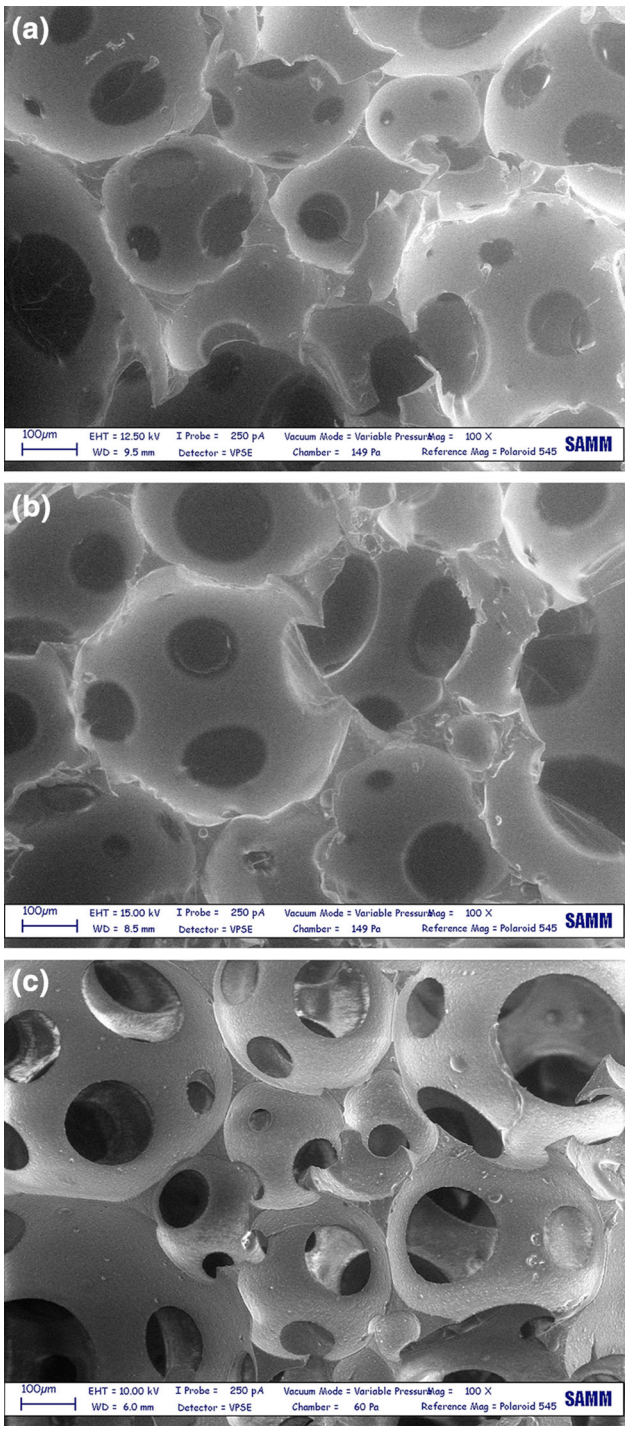

Fig. 2 Representative SEM images of the surface morphology of polyurethane foam samples: *ns* (**a**), and *pl* (**b**) and *oz* (**c**) sterilized. *Scale bar* 100 μm

N–H stretching, observed for not sterilized PU foam (3310 cm^{-1}, Fig. 5a), was not detectable. Furthermore, the *oz* spectrum presented in the carbonyl group region (at about 1780 cm^{-1}) a peak not observed in the spectra of the other samples, and did not show the CH_2 *bending* peak (1455 cm^{-1}, Fig. 5b).

To investigate possible change in phase separation onto the PU foam samples after sterilization, a height analysis of selected peaks (Table 2) was performed to provide a useful comparison among the effects of the two sterilization methods. In fact, ATR-FTIR is particularly useful to detect phase separation onto the surface of PU samples, as well as modification or formation of new chemical bonds by a degradation process. The obtained height ratios and their percent variations after plasma and ozone sterilization are reported in Table 4. After plasma treatment, the peak height ratios related to hard segments (3310, 1730, and 1703 cm^{-1}) showed a noticeable decrease (−76 % for N–H stretching and −74 % for non-hydrogen bonded carbonyls) and a slight decrease (−4 %) for the ratio related to free urethane carbonyls. Because the ratio between non-hydrogen-bonded and free urethane carbonyls changed hardly in respect to the control (i.e., $H_{1730}/H_{1703} = +324$ %), it can be assumed a greater phase separation on these samples, with a rearrangement of hydrogen bonds, confirmed also by the high increase of soft segments (+134 % for ether bonds). The ozone sterilization caused a noticeable change in all the considered peak ratios, related either to hard and soft segments. The great increase of both H-bonded NH and urethane carbonyls, the simultaneous increase of hydrogen-bonded carbonyls and the absence of some peaks observed in the IR spectrum of the not sterilized foam (i.e. CH_2 bending at 1455 cm^{-1}), indicate that the material degradation after ozone sterilization was homogeneous in its domain structure.

3.4 Mechanical characterization

Figure 6 shows representative hysteresis cycle curves of *ns*, *pl* and *oz* specimens obtained by uniaxial compressive tests, in wet conditions.

The σ/ε curves qualitatively follow the same trend, but for the ozone sterilized PU foam differences in the collapse part of the curve and in the maximum stress value (*i.e.* stress at 50 % deformation) can be observed. This was quantitatively verified by the analysis of the considered compressive mechanical parameters (Table 5).

By the fact, the compressive mechanical characterization performed in wet conditions on the sterilized samples showed mechanical parameters similar ($P > 0.05$) to those reported for not sterilized ones, except for the value of m and $\sigma_{50\ \%}$ of *oz*, that are significatively lower ($P < 0.05$) than the values shown by *ns* and *pl* specimens. This result may be related to the higher porosity and water uptake detected after ozone sterilization, that can influence the collapse modulus (m) and the maximum stress value ($\sigma_{50\ \%}$). In addition, the values of the

Table 3 Physico-morphological properties of *ns*, *pl* and *oz* samples

Sample	Density (g/cm^3)	Open porosity (%)	Average pore size (μm)
ns	0.113 ± 0.004	87.13 ± 1.00	310 ± 12
pl	0.115 ± 0.002	86.24 ± 0.66	291 ± 7
oz	0.113 ± 0.035	85.24 ± 1.04	222 ± 14

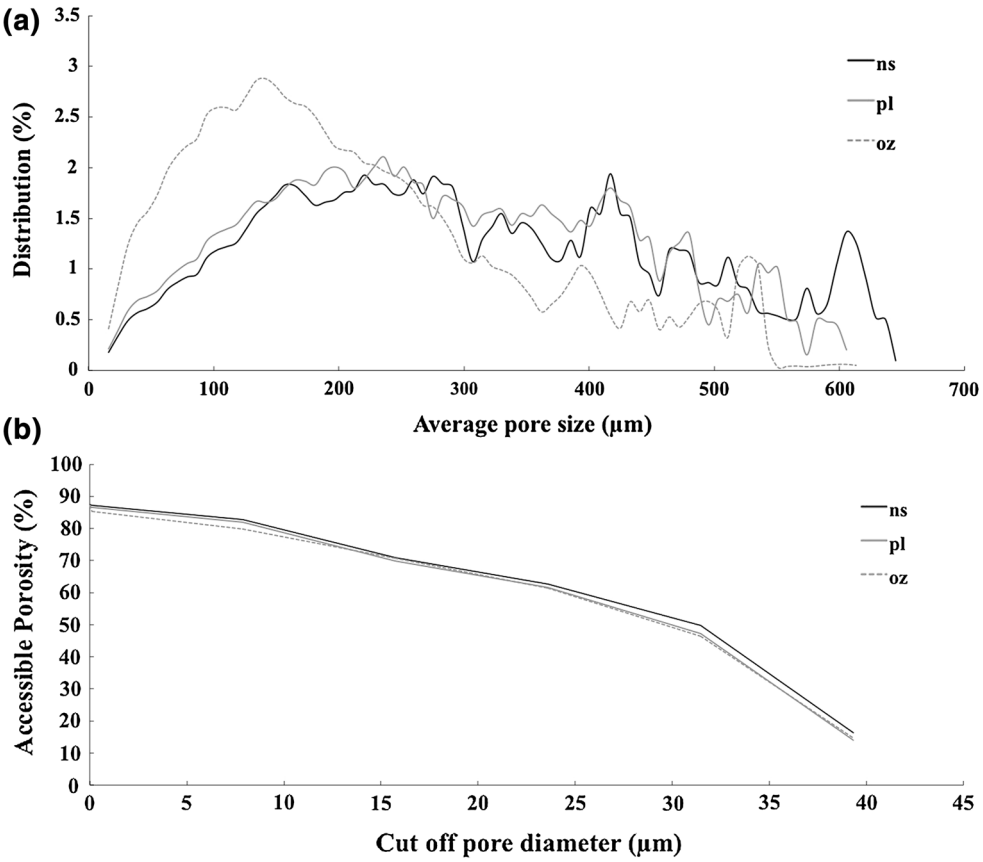

Fig. 3 Average pore size distribution of *ns*, *pl* and *oz* samples as obtained by micro-CT analysis (**a**); pore interconnection trends in terms of accessible porosity at different cut off pore diameter for *ns*, *pl* and *oz* PU foam samples (**b**)

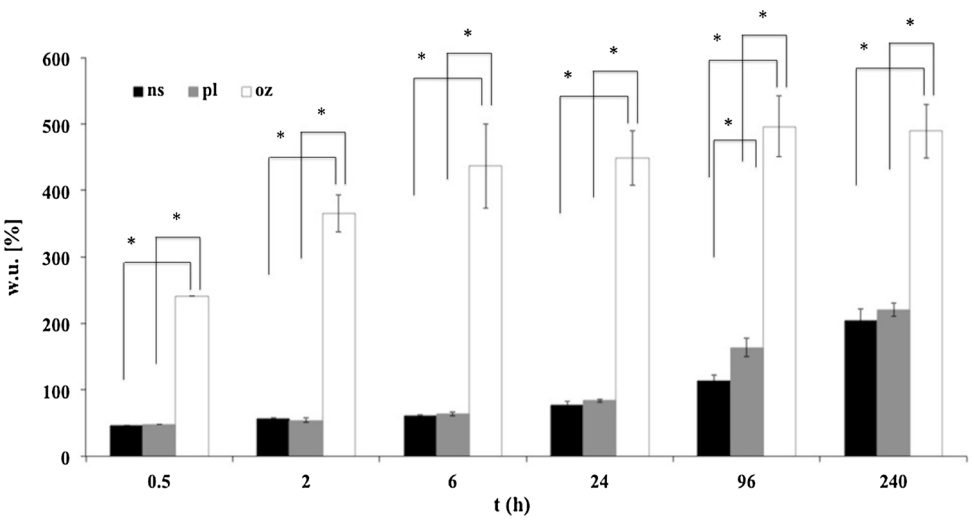

Fig. 4 Water uptake % of *ns*, *pl* and *oz* samples. $*P < 0.05$

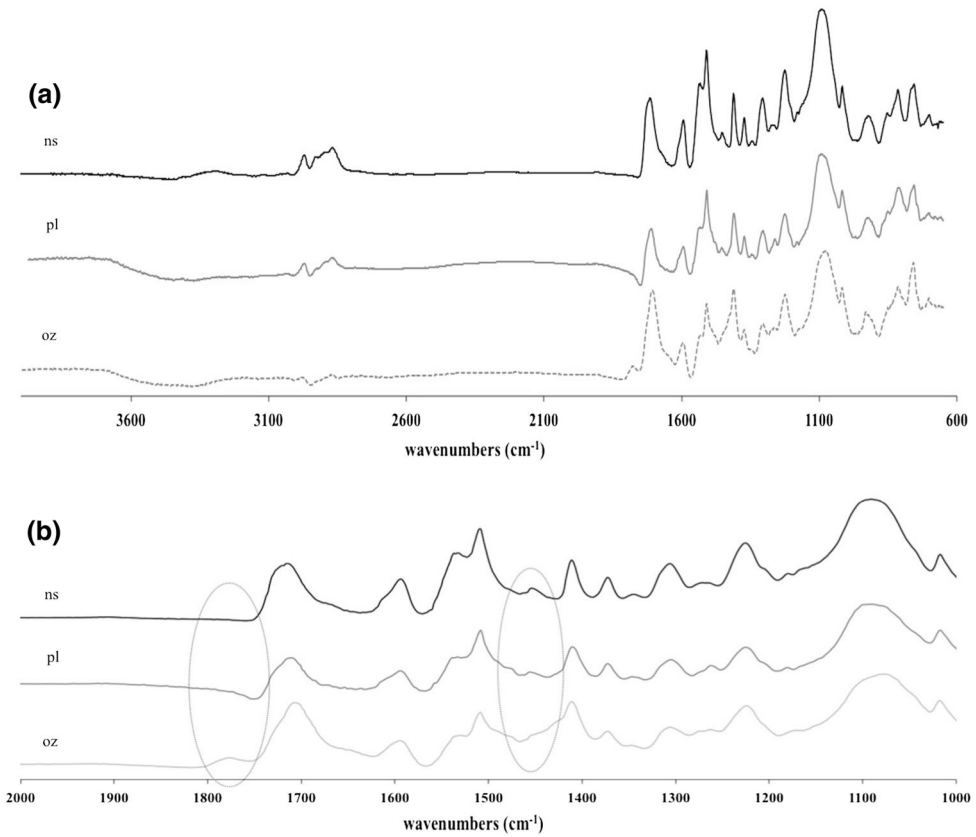

Fig. 5 **a** ATR-FT-IR spectra of the not sterilized (*ns*), plasma (*pl*) and ozone (*oz*) sterilized PU foam in the range 4000–600 cm^{-1}; **b** ATR-FT-IR spectra insight of image a, in the range 2000–1300 cm^{-1} (the peaks not observed in all the spectra are highlighted)

Table 4 Results of ATR-FTIR peak height analysis (in brackets: percentage variations versus reference peak of the control unsterilized foam)

PU foam	H_{3310}/H_{1597}	H_{1730}/H_{1597}	H_{1703}/H_{1597}	H_{1100}/H_{1597}
Control	0.14 ± 0.01	0.61 ± 0.10	1.33 ± 0.04	1.29 ± 0.50
Plasma	0.03 ± 0.01 (−76 %)	0.16* (−74 %)	1.28 ± 0.85 (−4 %)	3.00 ± 0.40 (+134 %)
Ozone	0.22* (+58 %)	n.d.	1.97 ± 0.29 (+48 %)	1.92 ± 0.26 (+49 %)

* Analysis performed only for the spectra presenting the specific band considered

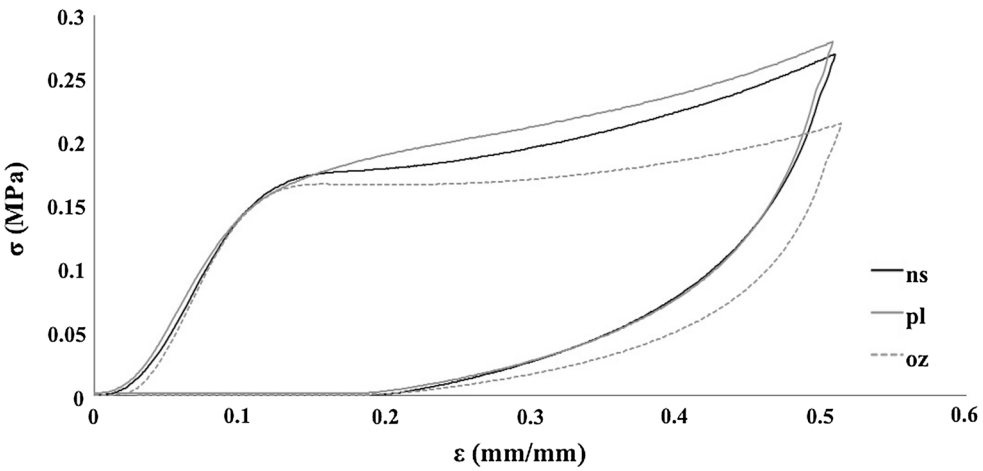

Fig. 6 Representative stress–strain curves of *ns*, *pl* and *oz* sterilized specimens

Table 5 Compressive mechanical properties of *ns*, *pl* and *oz* samples

Sample	E (MPa)	m (MPa)	$\sigma_{10\ \%}$ (MPa)	σ' (MPa)	ε' (mm/mm)	$\sigma_{50\ \%}$ (MPa)	Hysteresis area (J cm^{-3})
ns	2.04 ± 0.05	0.17 ± 0.01	0.14 ± 0.01	0.16 ± 0.01	0.11 ± 0.01	0.270 ± 0.001	0.066 ± 0.001
pl	2.06 ± 0.15	0.18 ± 0.06	0.15 ± 0.01	0.17 ± 0.01	0.11 ± 0.01	0.280 ± 0.002	0.073 ± 0.003
oz	1.85 ± 0.59	0.04 ± 0.02	0.13 ± 0.03	0.17 ± 0.01	0.12 ± 0.04	0.220 ± 0.010	0.062 ± 0.002

hysteresis area are significantly different ($P < 0.05$) after the sterilization, both with plasma and ozone. In particular, *oz* samples showed also a significantly lower ($P < 0.05$) hysteresis area than *pl* ones, related to the decrease of the $\sigma_{50\ \%}$ value.

3.5 In vitro cytotoxicity test

In vitro cytotoxicity test was performed on EMEM extracts previously put in contact with *ns*, *pl* and *oz* samples for 3 and 7 days. Figure 7 shows the absorbance values of Alamar Blue reduced by MG63 cells cultured in the presence of material extracts.

The values of reduced Alamar Blue indicated a good MG63 cell viability for cells cultured in contact with the extracts at both time points (3 and 7 days). Considering the 3 days eluates, a significant difference ($P < 0.05$) was observed only for *oz vs. ns* samples. In the case of the 7 days eluates, significant differences ($P < 0.05$) were detected between both *pl* and *oz* samples and not sterilized ones; a lower value of reduced Alamar Blue was observed for plasma sterilized samples, although this value (about 70 %) was still associated to a good cell viability. The average values of reduced Alamar Blue for the 3 days eluates were in general higher if compared to the values obtained for the 7 days eluates for all the considered samples, however this difference was statistically significant ($P < 0.05$) only for plasma-sterilized samples, due to the cell viability decrease at 7 days.

4 Discussion

Plasma and ozone sterilizations are recent technologies that could overcome the limitations of the sterilization methods traditionally used in the clinical practice for biomedical devices (*e.g.* ethylene oxide and γ rays). The operating conditions of these techniques, primarily the low temperature and the absence of toxic residuals, make them appealing for the use with polymeric materials. Furthermore, their non-toxic by-products (*i.e.* water and oxygen) make these techniques safe for operators and allow the immediate use of the device after sterilization, without the degassing period required, for example, after EtOx sterilization. It has to be noticed that the degassing phase could be extremely long for porous materials (i.e. up to 14 days) to assure the complete removal of the gas, then delaying their use.

Despite the great advantages of these techniques, the highly reactive sterilizing agent (in particular ozone) can cause serious modifications on the materials properties [44]. Therefore, a careful morphological, chemico-physical, mechanical and biological characterization of the materials after the sterilization process is mandatory. In addition, the effects of a specific sterilization technique can be completely different on compact materials (*i.e.* films) with respect to porous structures, that present a much larger surface area/volume ratio exposed to the sterilizer agent. This aspect, slightly discussed in the scientific literature, is particularly relevant for scaffold to be used in tissue engineering.

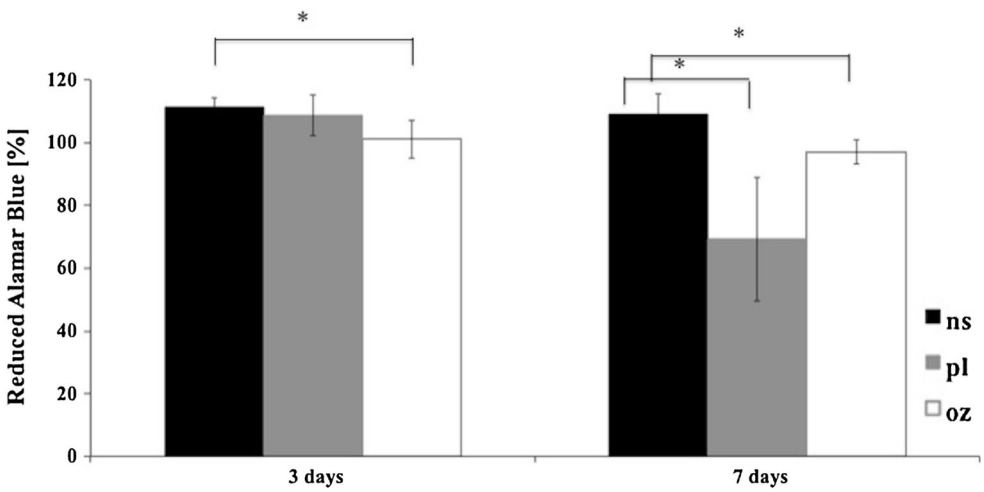

Fig. 7 Values of Alamar Blue reduced by MG63 cells cultured in contact with *ns*, *pl*, and *oz* sample eluates at 3 and 7 days. All the values are expressed as percentage versus the positive control (i.e. cells cultured in EMEM on TCPs wells). *$P < 0.05$

4.1 Effects on morphological properties

The results obtained by micro CT and the qualitative SEM observations indicate that plasma sterilization does not significantly affect the morphological properties of the PU foam. On the contrary, the ozone sterilization causes the formation of new small pores, with diameter in the range 100–150 μm (about +10 % if compared to not sterilized or plasma sterilized foam), thus leading to a decrease of the average pore size. The newly-formed pores do not increase the overall pore interconnection, as shown by open porosity values and pores interconnection trends, since they do not affect microporosity (up to 40 μm), that is mainly related to the presence of channels and interconnections between adjacent pores. Other studies [23, 34] analyzed the effects of plasma and ozone sterilization on shape memory polyurethane foams, observing an increase of open porosity after both sterilization procedures, due to the low pressure (i.e. 54–67 Pa) reached during the sterilization process [36]. On the contrary, the PU foam tested in the present work, having a higher value of open porosity (more than 85 %) compared to the SMP foams (21–59 %) [23], was less affected by the low pressure level of the sterilization cycle. In addition, the PU foam studied in this work presents a cross-linked structure that can be more resistant than the not cross-linked SMP foams to the effect of the low pressure applied during the sterilization cycle.

4.2 Effects on chemico-physical properties

The results obtained by ATR-FT-IR characterization after sterilization indicate, in agreement with the scientific literature [34, 36, 45], a degradation of the polyurethane foam, strongly affecting the IR bands related to ether peak [42]. The ozone sterilization affects also the absorption bands related to the carbonyl group, thus indicating phase separation and rearrangement of the hydrogen bonds at the surface. This effect is related to the high reactivity and oxidative property of the sterilizing agents used in plasma and ozone sterilization, *i.e.* hydrogen peroxide and ozone. In particular, the latter is a very reactive compound that can strongly react with the functional group present in the polyurethane structure, causing the formation of OH and radical groups and oxidative attack on the soft segments [27, 34]. Furthermore, hydroxyl radicals act as initiators of the poly(ether urethanes) oxidation process, causing surface pitting [46]. In the research work of Andrews et al. [27] electrospun Tecoflex® scaffolds were sterilized by UV-plasma sterilization, treating each side of the mat with UV-induced ozone for 20 s by the use of a UV-ozone sterilization unit. The oxidation of the material observed after the sterilization process was related to the decrease of surface roughness detected by atomic force microscopy [27].

Surface oxidation of the tested PU foam after sterilization was also visually confirmed by a strong yellowing of the samples, more pronounced after ozone sterilization. The oxidation of the sterilized PU foam, by ozone in particular, is confirmed also by the water uptake kinetics, where the modifications of the surface chemistry lead to an increase in PU foam hydrophilicity [36] due to material oxidation, thus increasing the water uptake value.

4.3 Effects on mechanical properties

The proposed PU foam combines an optimal morphological structure (*i.e.* high open porosity and interconnection) with good mechanical compressive properties in wet condition, if compared to other PU porous structures proposed as scaffolds for tissue engineering [1, 5].

The effects of sterilization on PU foam mechanical properties were not so marked as detected in case of the chemico-physical properties, especially for plasma sterilization. Considering ozone sterilization, the strong influence on the PU foam chemico-physical properties can be related to the significant decrease of collapse modulus and maximum stress values with respect to the not sterilized specimens. Therefore, the modification of the mechanical properties after ozone sterilization is imputable to a combined effect of material oxidation and degradation together with the presence of newly formed pores, that can lead to a decrease of the compressive strength of the material. In fact, the degradation caused by ozone can affect not only the foam surface, causing phase separation and rearrangement of the hydrogen bonds, but it modifies in some extent the bulk properties of the materials (*i.e.* mechanical properties). In addition, the surface exposed to sterilization in a porous structure is significantly higher than that of a compact structure having the same size, due to the presence of the pores. Therefore, the surface modification occurring after sterilization, in particular by ozone, can be stronger for the higher surface in contact with the sterilizing agent. At the same time, the decrease of the mechanical properties after ozone sterilization can be caused also by the synergistic effect of the increased water uptake, making the foam more flexible.

4.4 Effects on in vitro cytotoxicity

The sterilization process can modify so deeply the surface and bulk properties of a polymeric material to negatively influence its cytocompatibility and biocompatibility.

The good in vitro cytocompatibility of the proposed PU foam was already demonstrated in previous in vitro studies [13, 15–17]. In this work, we investigated the in vitro cytotoxicity of PU foam after sterilization, mainly to evaluate the possible release of cytotoxic low molecular weight products due to the sterilization process.

The data obtained by the in vitro cytotoxicity tests indicate that plasma and ozone sterilization do not evoke the release of cytotoxic products or cytotoxic effects of the polyurethane foams, as cell viability values were satisfying at considered time points. In fact, both at 3 and 7 days after plasma and ozone sterilization, the reduced Alamar Blue reached values over 70 %, indicating a good cell viability. Our results on plasma sterilized PU foam confirm those obtained by De Nardo et al. [23, 34] on SMP polyurethane foams sterilized by plasma. In fact, they did not observed any cytotoxic effects on L929 murine fibroblast cell line and, by in vitro cytocompatibility assay, they assessed a good cell interaction after 7 days of culture. However, the Authors did not perform direct in vitro tests on SMP sterilized by ozone, as a release of low molecular weight products from the ozone sterilized SMP foams was verified by high performance liquid chromatography [34].

5 Conclusions

In this work we demonstrated that plasma sterilization (Sterrad® method) can be a valid technique for the sterilization of the proposed polyurethane foam as, despite the modifications in phase separation observed by IR analysis, it does not cause any alteration in its physico-morphological and mechanical properties. In the case of ozone sterilization, a major effect of the sterilizing agent, more active than hydrogen peroxide, on the material bulk properties was observed. The formation of new small pores, together with an increase in material hydrophilicity, was detected. Even though degradation occurs after sterilization, both plasma and ozone sterilization did not affect PU foam in vitro cytotoxicity, as they did not cause the release of toxic products.

Ozone sterilization, alike Sterrad® method already used worldwide in several hospitals, appears promising for a clinical use, although the results obtained in this work suggest that the setting up of a specific sterilization protocol, controlling dose and time of exposition, is needed before its use for sterilizing polyurethane scaffolds and, overall, porous structures. Furthermore, a complete characterization regarding the in vitro cytocompatibility after sterilization of the PU foam is required to validate the use of the two sterilization process here tested.

Studies such as the one here proposed can help in understanding the effects of sterilization procedures on porous polymeric scaffolds for tissue engineering and, viceversa, the influence of the scaffold morphology, porosity in particular, on the effects of sterilization. Further researches should be performed to select the optimal sterilization technique for porous scaffolds for advanced applications in regenerative medicine.

Acknowledgments Authors would like to thank Prof. M. Nava (IRCCS Istituto Nazionale per lo Studio e la Cura dei Tumori, Milan, Italy) for Plasma Sterilization treatment and Dr. R. Marchand and Prof. L'H. Yahia (Montréal, QC, Canada) for Ozone Sterilization.

References

1. Gogolewski S, Gorna K, Zaczynska E, Czarny A. Structure-property relations and cytotoxicity of isosorbide-based biodegradable polyurethane scaffolds for tissue repair and regeneration. J Biomed Mater Res A. 2008;85(2):456–65.
2. Lamba NM, Woodhouse K, Cooper S. Polyurethanes in biomedical applications. Boca Raton: CRC Press; 1998.
3. Lelah MD, Cooper JL. Polyurethanes in Medicine. Boca Raton: CRC Press; 1987.
4. Guelcher SA. Biodegradable polyurethanes: synthesis and applications in regenerative medicine. Tissue Eng Part B Rev. 2008;14(1):3–17.
5. Gorna K, Gogolewski S. Preparation, degradation, and calcification of biodegradable polyurethane foams for bone graft substitutes. J Biomed Mater Res. 2003;67A(3):813–27.
6. Bonzani IC, Adhikari R, Houshyar S, Mayadunne R, Gunatillake P, Stevens MM. Synthesis of two-component injectable polyurethanes for bone tissue engineering. Biomaterials. 2007;28(3):423–33.
7. Zhang J, Doll BA, Beckman EJ, Hollinger JO. A biodegradable polyurethane–ascorbic acid scaffold for bone tissue engineering. J Biomed Mater Res A. 2003;67(2):389–400.
8. Gunatillake PA, Adhikari R. Biodegradable synthetic polymers for tissue engineering. Eur Cell Mater. 2003;5:1–16.
9. Werkmeister JA, Adhikari R, White JF, Tebb TA, Le TP, Taing HC, Mayadunne R, Gunatillake PA, Danon SJ, Ramshaw JA. Biodegradable and injectable cure-on-demand polyurethane scaffolds for regeneration of articular cartilage. Acta Biomater. 2010;6(9):3471–81.
10. De Groot JH. Polyurethane scaffolds for meniscal tissue regeneration. Med Device Technol. 2005;16(7):18–20.
11. Heijkants RG, Van Calck RV, De Groot JH, Pennings AJ, Schouten AJ, van Tienen TG, Ramrattan N, Buma P, Veth RP. Design, synthesis and properties of a degradable polyurethane scaffold for meniscus regeneration. J Mater Sci Mater Med. 2004;15(4):423–7.
12. Farè S, Petrini P, Tanzi MC. 3-D polyurethane scaffolds for bone reconstruction. EUROMAT 2001. Biomaterials. 2001;6:1–7 ISBN 88-85298-39-7.
13. Tanzi MC, Fare S, Petrini P, Tanini A, Piscitelli E, Zecchi Orlandini S, Brandi ML. Cytocompatibility of polyurethane foams as biointegrable matrices for the preparation of scaffolds for bone reconstruction. J Appl Biomater Biomech. 2003;1(1):58–66.
14. Fare S, Petrini P, Tanzi MC, Bigi A, Roveri N. Biointegrable 3-D polyurethane/a-TCP composites for bone reconstruction. In: Mantovani D, editor. Advanced materials for biomedical application. Montréal: Canadian Institute of Mining, Metallurgy and Petroleum; 2002. p. 17–26.
15. Fassina L, Visai L, Asti L, Benazzo F, Speziale P, Tanzi MC, Magenes G. Calcified matrix production by SAOS-2 cells inside a polyurethane porous scaffold, using a perfusion bioreactor. Tissue Eng. 2005;11(5–6):685–700.
16. Zanetta M, Quirici N, Demarosi F, Tanzi MC, Rimondini L, Farè S. Ability of polyurethane foams to support cell proliferation and the differentiation of MSCs into osteoblasts. Acta Biomater. 2009;5(4):1126–36.
17. Bertoldi S, Farè S, Denegri M, Rossi D, Haugen HJ, Parolini O, Tanzi MC. Ability of polyurethane foams to support placenta-

derived cell adhesion and osteogenic differentiation: preliminary results. J Mater Sci Mater Med. 2010;21(3):1005–11.
18. Simmons A. Sterilisation of medical devices. Business Briefing: Medical Device Manufacturing and Technology; 2004. p. 1–4.
19. Simmons A, Hyvarinen J, Poole-Warren L. The effect of sterilisation on a poly(dimethylsiloxane)/poly(hexamethylene oxide) mixed macrodiol-based polyurethane elastomer. Biomaterials. 2006;27(25):4484–97.
20. Hirata N, Matsumoto K, Inishita T, Takenaka Y, Suma Y, Shintani H. Gamma-ray irradiation, autoclave and ethylene oxide sterilization to thermosetting polyurethane: sterilization to polyurethane. Radiat Phys Chem. 1995;46(3):377–81.
21. Haugen HJ, Gerhardt LC, Will J, Wintermantel E. Biostability of polyether-urethane scaffolds: a comparison of two novel processing methods and the effect of higher gamma-irradiation dose. J Biomed Mater Res B. 2005;73(2):229–37.
22. Gorna K, Gogolewski S. The effect of gamma radiation on molecular stability and mechanical properties of biodegradable polyurethanes for medical applications. Polym Degrad Stab. 2003;79(3):465–74.
23. De Nardo L, Alberti R, Cigada A, Yahia L, Tanzi MC, Farè S. Shape memory polymer foams for cerebral aneurysm reparation: effects of plasma sterilization on physical properties and cytocompatibility. Acta Biomater. 2009;5(5):1508–18.
24. Gorna K, Gogolewski S. Molecular stability, mechanical properties, surface characteristics and sterility of biodegradable polyurethanes treated with low-temperature plasma. Polym Degrad Stab. 2003;79(3):475–85.
25. Dal Prà I, Petrini P, Charini A, Bozzini S, Farè S, Armato U. Silk fibroin-coated three-dimensional polyurethane scaffolds for tissue engineering: interactions with normal human fibroblasts. Tissue Eng. 2003;9(6):1113–21.
26. Laschke MW, Strohe A, Scheuer C, Eglin D, Verrier S, Alini M, Pohlemann T, Menger MD. In vivo biocompatibility and vascularization of biodegradable porous polyurethane scaffolds for tissue engineering. Acta Biomater. 2009;5(6):1991–2001.
27. Andrews KD, Hunt JA, Black RA. Effects of sterilisation method on surface topography and in vitro cell behaviour of electrostatically spun scaffolds. Biomaterials. 2007;28(6):1014–26.
28. Grad S, Lee CR, Gorna K, Gogolewski S, Wimmer MA, Alini M. Surface motion upregulates superficial zone protein and hyaluronan production in chondrocyte-seeded three-dimensional scaffolds. Tissue Eng. 2005;11(1–2):249–56.
29. Kim SS, Park MS, Gwak SJ, Choi CY, Kim BS. Accelerated bonelike apatite growth on porous polymer/ceramic composite scaffolds in vitro. Tissue Eng. 2006;12(10):2997–3006.
30. Van Minnen B, Van Leeuwen MBM, Stegenga B, Zuidema J, Hissink CE, Van Kooten TG, Bos RRM. Short-term in vitro and in vivo biocompatibility of a biodegradable polyurethane foam based on 1,4-butanediisocyanate. J Mater Sci Mater Med. 2005; 16(3):221–7.
31. Wolchok JC, Brokopp C, Underwood CJ, Tresco PA. The effect of bioreactor induced vibrational stimulation on extracellular matrix production from human derived fibroblasts. Biomaterials. 2009;30(3):327–35.
32. Haugen HJ, Brunner M, Pellkofer F, Aigner J, Will J, Wintermantel E. Effect of different γ-irradiation doses on cytotoxicity and material properties of porous polyether-urethane polymer. J Biomed Mater Res B. 2007;80(2):415–23.
33. Woźniak P, Bil M, Ryszkowska J, Wychowański P, Wróbel E, Ratajska A, Hoser G, Przybylski J, Kurzydłowski KJ, Lewandowska-Szumieł M. Candidate bone-tissue-engineered product based on human-bone-derived cells and polyurethane scaffold. Acta Biomater. 2010;6(7):2484–93.
34. De Nardo L, Moscatelli M, Silvi F, Tanzi MC, Yahia L, Farè S. Chemico-physical modifications induced by plasma and ozone sterilizations on shape memory polyurethane foams. J Mater Sci Mater Med. 2010;21(7):2067–78.
35. Ganta SR, Piesco NP, Long P, Gassner R, Motta LF, Papworth GD, Stolz DB, Watkins SC, Agarwal S. Vascularization and tissue infiltration of a biodegradable polyurethane matrix. J Biomed Mater Res A. 2003;64A(2):242–8.
36. Lerouge S, Tabrizian M, Wertheimer MR, Marchand R, Yahia L. Safety of plasma-based sterilization: surface modifications of polymeric medical devices induced by Sterrad® and Plazlyte™ processes. Biomed Mater Eng. 2002;12(1):3–13.
37. Dufresne S, Leblond H, Chaunet M. Relationship between lumen diameter and length sterilized in the 125L ozone sterilizer. Am J Infect Control. 2008;36(4):291–7.
38. Moore MJ, Jabbari E, Ritman EL, Lu LC, Currier BL, Windebank AJ, Yaszemski MJ. Quantitative analysis of interconnectivity of porous biodegradable scaffolds with micro-computed tomography. J Biomed Mater Res A. 2004;71A(2):258–67.
39. Wu Y, Sellitti C, Anderson JM, Hiltner A, Lodoen GA, Payet CR. An FTIR-ATR investigation of in vivo poly(ether urethane) degradation. J Appl Polym Sci. 1992;46(2):201–11.
40. Meijs GF, McCarthy SJ, Rizzardo E, Chen Y, Chatelier RC, Brandwood A, Schindhelm K. Degradation of medical-grade polyurethane elastomers: the effect of hydrogen peroxide in vitro. J Biomed Mater Res. 1993;27(3):345–56.
41. Faré S, Petrini P, Motta A, Cigada A, Tanzi MC. Synergistic effects of oxidative environments and mechanical stress on in vitro stability of polyetherurethanes and polycarbonateurethanes. J Biomed Mater Res. 1999;45(1):62–74.
42. Schubert MA, Wiggins MJ, Schaefer MP, Hiltner A, Anderson JM. Oxidative biodegradation mechanisms of biaxially strained poly(etherurethane urea) elastomers. J Biomed Mater Res. 1995; 29(3):337–47.
43. Schubert MA, Wiggins MJ, Anderson JA, Hiltner A. The effect of strain state on the biostability of a poly(etherurethane urea) elastomer. J Biomed Mater Res. 1997;35(3):319–28.
44. Ratner BD, Hoffman AS, Schoen FJ, Lemons JE, editors. Biomaterials science: an introduction to materials in medicine. 3rd ed. San Diego: Elsevier Academic Press; 2012.
45. Moisan M, Barbeau J, Moreau S, Pelletier J, Tabrizian M, Yahia LH. Low-temperature sterilization using gas plasmas: a review of the experiments and an analysis of the inactivation mechanisms. Int J Pharm. 2001;226(1–2):1–21.
46. Christenson EM, Anderson JM, Hiltner A. Oxidative mechanisms of poly(carbonate urethane) and poly(ether urethane) biodegradation: in vivo and in vitro correlations. J Biomed Mater Res A. 2004;70A(2):245–55.